FOI-R--0838--SE
March 2003
ISSN 1650-1942
Scientific report

Andreas Rung

Modelling photonic band structures

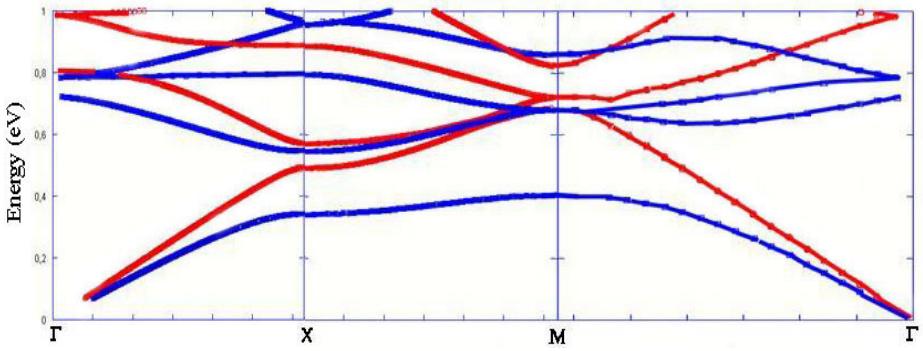

Sensor Technology
SE-581 11 Linköping

SWEDISH DEFENCE RESEARCH AGENCY

Sensor Technology
P.O. Box 1165
SE-581 11 Linköping

FOI-R--0838--SE

March 2003

ISSN 1650-1942

Scientific report

Andreas Rung

Modelling photonic band structures

Issuing organization FOI – Swedish Defence Research Agency Sensor Technology P.O. Box 1165 SE-581 11 Linköping	**Report number, ISRN** FOI-R--0838--SE	**Report type** Scientific report
	Research area code 6. Electronic Warfare	
	Month year March 2003	**Project no.** E3033
	Customers code 5. Commissioned Research	
	Sub area code 62 Stealth Technology	
Author/s (editor/s) Andreas Rung	**Project manager** Tomas Hallberg	
	Approved by	
	Sponsoring agency Swedish Armed Forces	
	Scientifically and technically responsible Tomas Hallberg	
Report title Modelling photonic band structures		

Abstract (not more than 200 words)

A software package has been used to calculate and compare the photonic band structures for two structures: one structure consisting of dielectric cylinders in a square lattice, and the inverse; a structure with air columns in a dielectric matrix. The appearance of and differences between TE- and TM-gaps are compared. Transmittance for normal incidence was calculated for both structures, with a material thickness of 8 μm. The photonic band gap width at the X-point of the band structure as a function of the packing fraction of cylinders was investigated for the two cases.

Keywords Photonic band gap, modelling, IR	
Further bibliographic information	**Language** English
ISSN 1650-1942	**Pages** 29 p.
	Price acc. to pricelist

Utgivare Totalförsvarets Forskningsinstitut - FOI Sensorteknik Box 1165 581 11 Linköping	**Rapportnummer, ISRN** FOI-R--0838--SE	**Klassificering** Vetenskaplig rapport
	Forskningsområde 6. Telekrig	
	Månad, år Mars 2003	**Projektnummer** E3033
	Verksamhetsgren 5. Uppdragsfinansierad verksamhet	
	Delområde 62 Signaturanpassning	
Författare/redaktör Andreas Rung	**Projektledare** Tomas Hallberg	
	Godkänd av	
	Uppdragsgivare/kundbeteckning Försvarsmakten	
	Tekniskt och/eller vetenskapligt ansvarig Tomas Hallberg	
Rapportens titel (i översättning) Modellering av fotonbandstrukturer		

Sammanfattning (högst 200 ord)

Ett programpaket har använts för att beräkna och jämföra fotonbandstrukturerna för två material: ett bestående av dielektriska cylindrar i ett kvadratiskt gitter, och inversen av detta – ett material bestående av cylindriska lufthål i en dielektrisk matris. Uppkomsten av och skillnaderna mellan TE- och TM-gap har jämförts. Transmittans för normalt infall beräknades för båda materialen med tjockleken 8 μm. Fotonbandgapets bredd vid bandstrukturens X-punkt har beräknats som funktion av cylindrarnas packningsgrad för de båda materialen.

Nyckelord Fotonbandgap, modellering, IR	
Övriga bibliografiska uppgifter	**Språk** Engelska
ISSN 1650-1942	**Antal sidor:** 29 s.
Distribution enligt missiv	**Pris: Enligt prislista**

Table of contents

1. Introduction

A *photonic crystal* is a periodically arranged structure consisting of at least two materials with different optical properties [1]. Typically both materials are dielectric, i.e. non-absorbing, one is a high index material and the other is a low index material, such as air or a polymer. The ratio of the two indices, n_H/n_L is sometimes used as a parameter to specify this property. The translational symmetry is such that the repeat distance is of the same order of magnitude as the wavelength of the light that the crystal is designed to control. An alternative short characterization of a photonic crystal is *a generalized diffraction grating*. It is thus not surprising that it can be used to influence the behaviour of an incoming light-beam.

The characteristic property of a photonic crystal is that an electromagnetic wave propagating in the crystal obeys a non-trivial dispersion relation

$$h\nu = f(\mathbf{K}) \qquad (1)$$

which will be discussed in more detail below.

An analogy to the dispersion relation (1) is the energy band structure for valence electrons in an ordinary crystal. The allowed states for electromagnetic waves in a photonic crystal can also be collected as branches of ν vs. **K**-curves, valid for different directions in the unit cell in wave-vector space, the Brillouin zone (BZ). Together these branches form a *photonic band structure*. It is typical for electronic band structures that they exhibit effects of symmetry, i.e. different behaviour in different symmetries and directions. The photonic bands also show diffraction effects near the limits of the BZ. These two effects are what was referred to as "non-trivial" above.

The feature that has attracted most attention for both kinds of band structures is the presence of *band gaps*, i.e. energy intervals within which electrons and electromagnetic waves respectively, cannot propagate inside the crystal. Physically this can be understood as an effect from imaginary **K**-values within the band gap. An imaginary **K** causes exponential damping of the wave as obvious from the expression for a plane wave:

$$\mathbf{E}(\mathbf{r},t) = \mathbf{E}_0 e^{i(\mathbf{K}\bullet\mathbf{r}-\omega t)} \qquad (2)$$

Within a few lattice constants of penetration into the photonic crystal, the incoming electro-magnetic wave is therefore effectively extinguished. If there exists an energy interval for

which **K** is imaginary for *all* angles of incidence and both polarizations, the band gap is additionally labelled *complete*. Complete band gaps appear for certain symmetries and if the index contrast is sufficiently large. Light with photon energy within the complete photonic gap will be totally reflected for any angles of incidence and state of polarization.

If the transmittance T(λ) = 0, then total reflection is equivalent to zero emittance, which can be understood as a consequence of the relation between bulk optical emittance and reflectance:

$$\varepsilon(\lambda) = 1 - R(\lambda) \qquad (3)$$

This equation can be used both at single wavelengths and suitably averaged over a wavelength interval.

Thus, for bulk photonic crystals with complete band gaps, zero emittance can be expected within the energy gap. Formally this effect can be expressed by the equation for the thermal excitance [2]:

$$M(\lambda,T) = \varepsilon(\lambda)\frac{2hc^2}{\lambda^5[\exp(\frac{hc}{k\lambda T}) - 1]} \qquad (4)$$

M is the emitted power per unit area and wavelength written as the product of the spectral emittance and the Planck function for blackbody excitance. Eq (4) shows clearly that if the spectral emittance ε(λ) =0 for one wavelength or a wavelength interval, then the thermal emission will vanish for these wavelengths.

This *selective low emittance* is the basis for the present project on signature management. It represents a development of the traditional method of using broad band reflectors to suppress thermal emission. The typical example of this conventional approach is a shiny metal surface, which is low-emitting from visible wavelengths through all of the thermal infrared. In other words, eq. 3 above is averaged over the λ-values 0.5-50 μm instead of just one IR band as in the selective case. There are some drawbacks with the broadband suppression. A shiny metal, as required for the low thermal emission, is not suitable in the visible. The broadband suppression will seriously impair the radiative cooling, which is important for hot stationary or slowly moving objects. The fact that metals are electrical conductors that completely

screen electromagnetic waves in the radar and microwave ranges excludes their use on various radomes.

In this work we shall discuss photonic crystals designed for suppressing thermal radiation in one of two wavelength regions, 3-5 μm and 8-13 μm, the infrared (IR) regions denoted as the two *atmospheric windows*. They are crucial since they correspond to the wavelength intervals where the atmosphere is transparent. In figure 1 the infrared transmission spectrum over 1.8 km of clear, relatively dry atmosphere is shown.

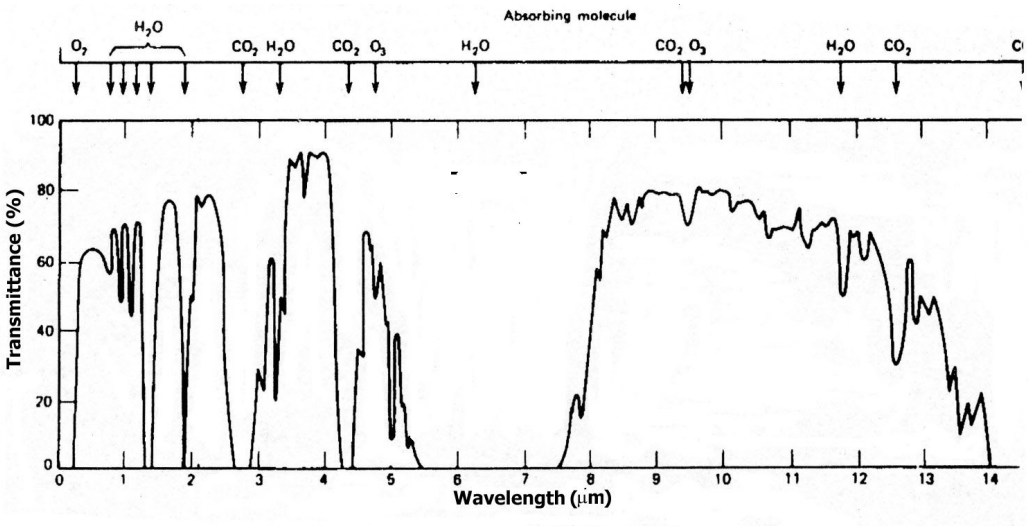

Fig. 1: The atmosphere absorbs infrared radiation due to the presence of gas molecules. The transmittance vs. wavelength is shown above, and the absorbing gas molecules are indicated above the graph. Cited from [3].

Figure 1 explains why the infrared seekers work within the two windows 3-5 and 8-13 μm. Going outside these ranges would only marginally increase the signal from the object, and strongly increase the noise of radiation from the atmosphere between the seeker and the object. The *choice* of window is partly dependent upon the temperature of the object. The peak position of blackbody curve, as obtained from (4), is at about 4 μm for T=450^{o}C and at 9 μm for 50^{o}C.

1.1 Signature Applications

Modern IR sensors in for example seeker missiles operating in either of the two atmospheric windows are highly sensitive, and therefore it is important for military vehicles to blend in with the background, in an IR perspective. One way to deal with this quite intricate problem is

to apply a low-emitting coating on the vehicle, thereby decreasing the IR signature to something equal to that of the terrain in which the vehicle operates. A thin layer [4] of a photonic band gap material is well suited for this purpose, since it can be tailored to be low emitting in either of the two regions where the IR missile seekers operate.

Intuitively, the IR appearance of the background is different depending on the environment, and therefore it is important to tailor the emission to values close to that of the terrain. As mentioned above, a bulk photonic crystal with a complete band gap will result in zero emittance – which is not optimal for signature reduction purposes. The background has also a wavelength-depending excitance according to (4).

$\varepsilon(\lambda)$ is in this case a complex material-dependent emittance function that depends on a more or less mixed terrain, more likely to be determined by data collected from IR measurements than by an analytical expression.

The optical performance of a signature-managing coating should, primarily for practical and economic reasons, be optimised to work in a wide area of terrains and also during different seasons of the year. In the visual range, the optimisation is difficult, if even possible because of the different terrain colours during a normal year. In the infrared, however, the optimization process can be performed by collecting IR data from the main terrain type and through calculating an average IR terrain signature it can be chosen which IR signature the vehicle should have.

Furthermore it is important to investigate the vehicles more carefully in terms of radiating parts. Exhaust pipes, vents, chimneys on boats, wheels and bands on tanks, the nose cone of an aircraft and engines are among the parts that will be heated during operation, and therefore in particular should be prepared with a low-emitting photonic band gap material.

2. Light dispersion in a solid

2. 1 Elements of Material Optics

On the length scale of the wavelength of light, the charge distribution of a solid is homogenous, and when the solid is excited by light, microscopic dipoles are created. The size of each dipole is small compared to the wavelength of the exciting electro-magnetic wave, which effectively means that a light wave creates an excitation averaged over a great number of dipoles. This average is quantified by the complex dielectric function, ε(ω), which gives the total dielectric displacement from the macroscopic polarization through the constitutive relation

$$\mathbf{D}(\omega) = \varepsilon_0 \mathbf{E}(\omega) + \mathbf{P}(\omega) = \varepsilon_0 \varepsilon(\omega) \mathbf{E}(\omega) \qquad (5)$$

In the case of photonic crystals, a different type of averaging is necessary, since the photonic crystal is inhomogeneous on a length scale comparable to the wavelength of the light. Averaging over a wavelength is therefore not applicable, but nevertheless effective medium theory (EMT) has been used to simplify the calculations of the optical performance of photonic crystals [5].

Returning to the formalism of optical excitation of a normal, homogeneous medium, we write the electromagnetic wave equation,

$$\nabla^2 \mathbf{E} = \mu_0 \frac{\partial^2 \mathbf{D}}{\partial t^2} \qquad (6)$$

in combination with the expression for the displacement given above and the equation for a plane electromagnetic wave, (2), gives a dispersion relation, i.e. ω as a function of the wave vector, K.

$$\omega^2 = \frac{c^2 K^2}{\varepsilon(\omega)} \qquad (7)$$

If we observe that ε(ω) is a complex quantity, we can take the square root of the above expression to obtain a linear equation relating ω to K:

$$\omega = \frac{c}{N} K \qquad (8)$$

where $N(\omega) = \sqrt{\varepsilon(\omega)}$ is the complex refractive index.

It is possible to express the dispersion graphically in an ω vs. K-diagram. In vacuum or in a non-dispersive medium, N is constant, which gives ω(**K**) vs. **K** as a straight line, sometimes named the *light line*. "Dispersion" often implies that the dielectric function, and hence the complex refractive index, varies with ω. This occurs in all solids. Nevertheless, some materials are non-dispersive within limited frequency ranges, and a straight line can be used.

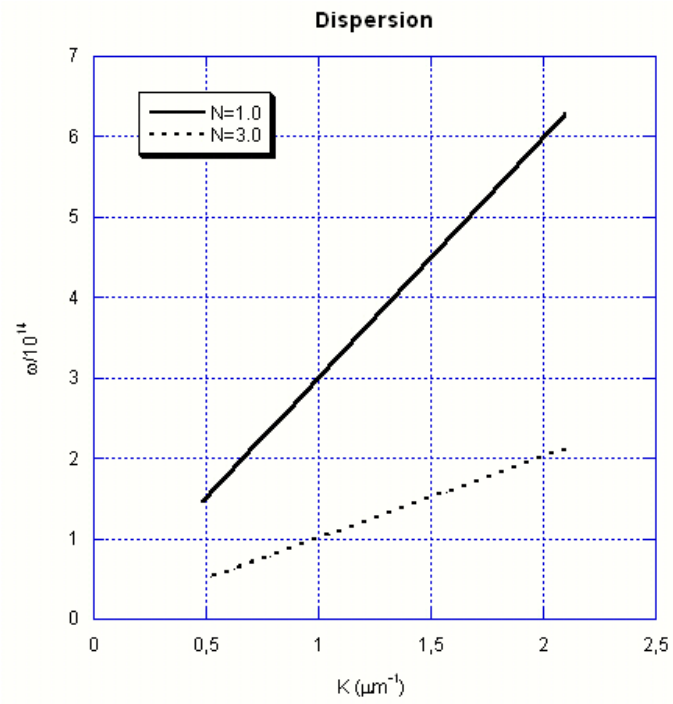

Fig. 2: An example of two linear dispersion curves; the solid line corresponds to N=1.0 and the dotted line to N=3.0.

2.2 Wave-vector space and the reciprocal lattice

We now return to the photonic crystal introduced above. For a photonic crystal, crystalline order is a key feature. Long range crystalline order is described by a repetition of one unit cell, which is described by three lattice translation vectors: $\mathbf{a}_1$, $\mathbf{a}_2$ and $\mathbf{a}_3$. Mutual orthogonality is not a must, neither that they have the same length. However, for two of the most common structures, the body-centred cubic (bcc) and the face-centred cubic (fcc) the lattice translation vectors are equally long:

$$a_1 = \frac{a}{2}(\hat{x}+\hat{y}-\hat{z}), a_2 = \frac{a}{2}(-\hat{x}+\hat{y}+\hat{z}), a_3 = \frac{a}{2}(\hat{x}-\hat{y}+\hat{z}) \qquad (9)$$

and

$$a_1 = \frac{a}{2}(\hat{x}+\hat{y}), a_2 = \frac{a}{2}(\hat{y}+\hat{z}), a_3 = \frac{a}{2}(\hat{x}+\hat{z}) \qquad (10)$$

respectively.

We now introduce the reciprocal space, or **k**-space, as referred to in solid state physics. The unit cell in the reciprocal space is defined by three vectors $\mathbf{b}_1$, $\mathbf{b}_2$ and $\mathbf{b}_3$:

$$b_i = 2\pi \frac{a_j \times a_k}{a_i \cdot (a_j \times a_k)} \qquad (11)$$

where the indices (i,j,k) = 1,2,3 through cyclic permutation. The **b**-vectors span a reciprocal unit cell, and all points in the reciprocal space can be reached through a reciprocal lattice vector $\mathbf{G}=x\mathbf{b}_1+y\mathbf{b}_2+z\mathbf{b}_3$ where (x,y,z) are integers. In reciprocal space the vectors have the dimension of inverse length. This implies that the wave-vectors **K** of light belong to reciprocal space.

The reciprocal version of the primitive unit cell is the first Brillouin zone (BZ), which is the minimum volume enclosed by planes intersecting the reciprocal vectors $\mathbf{G}_i$ from the origin to the nearest neighbouring reciprocal lattice points. Conventionally, the BZ has a set of symbols for points of high symmetry; e.g. Γ denotes the origin of the reciprocal representation of the unit cell. These symbols are basic for reading and interpreting both electronic and photonic band structures.

We shall use **K** as a general vector in the three-dimensional **k**-space. As mentioned above, **K** is a wave-vector. A band structure consists of $\omega(\mathbf{K})$-lines along the directions of highest symmetry in the reciprocal space. The long range symmetry in real space results in a long range symmetry also in the reciprocal space. Since all lattice points in reciprocal space can be reached by translations with reciprocal lattice vectors **G,** symmetry tells us that it is possible to collect all energy or frequency values within one BZ. This is named *the reduced zone scheme*. A band structure, electronic or photonic, is thus a representation of the dispersion, with various branches that have been translated into the first Brillouin zone.

3. Calculating a photonic band structure and the resulting optical properties

3.1 Calculating the band structure

An existing software package [6] has been used for calculating the photonic band structures. The overview of the formalism presented below is largely based on [7, 8].

The calculation of a photonic band structure is essentially a discretization of Maxwell's equations

$$\nabla \times \mathbf{E} = -\frac{\partial \mathbf{B}}{\partial t}, \quad \nabla \times \mathbf{H} = \frac{\partial \mathbf{D}}{\partial t} \tag{12}$$

which transformed into (ω, **k**)-space are

$$i\mathbf{k} \times \mathbf{E} = i\omega\mathbf{B}, \quad i\mathbf{k} \times \mathbf{H} = -i\omega\mathbf{D} \tag{13}$$

They can in turn be rewritten as components to obtain

$$\begin{aligned} k_y\mathbf{E}_z - k_z\mathbf{E}_y &= \omega\mathbf{B}_x \\ k_z\mathbf{E}_x - k_x\mathbf{E}_z &= \omega\mathbf{B}_y \\ k_x\mathbf{E}_y - k_y\mathbf{E}_x &= \omega\mathbf{B}_z \end{aligned} \quad \text{and} \quad \begin{aligned} k_y\mathbf{H}_z - k_z\mathbf{H}_y &= -\omega\mathbf{D}_x \\ k_z\mathbf{H}_x - k_x\mathbf{H}_z &= -\omega\mathbf{D}_y \\ k_x\mathbf{H}_y - k_y\mathbf{H}_x &= -\omega\mathbf{D}_z \end{aligned} \tag{14}$$

For small translations in **k**-space, the **k**-vector can be approximated using

$$\begin{aligned} \mathbf{k}_x &\approx (ia)^{-1}\left[\exp(ik_x a) - 1\right] \\ \mathbf{k}_y &\approx (ib)^{-1}\left[\exp(ik_y b) - 1\right] \\ \mathbf{k}_z &\approx (ic)^{-1}\left[\exp(ik_z c) - 1\right] \end{aligned} \tag{15}$$

where a, b and c are the cell dimensions in x-, y- and z direction respectively.

Inserting these approximations into the set of component equations (14), and Fourier transforming back to (**r**, t) space gives

$$\begin{aligned} (ib)^{-1}\left[\mathbf{E}_z(\mathbf{r}+\mathbf{b}) - \mathbf{E}_z(\mathbf{r})\right] - (ic)^{-1}\left[\mathbf{E}_y(\mathbf{r}+\mathbf{c}) - \mathbf{E}_y(\mathbf{r})\right] &= \omega\mathbf{B}_x(\mathbf{r}) \\ (ic)^{-1}\left[\mathbf{E}_x(\mathbf{r}+\mathbf{c}) - \mathbf{E}_x(\mathbf{r})\right] - (ia)^{-1}\left[\mathbf{E}_z(\mathbf{r}+\mathbf{a}) - \mathbf{E}_z(\mathbf{r})\right] &= \omega\mathbf{B}_y(\mathbf{r}) \\ (ia)^{-1}\left[\mathbf{E}_y(\mathbf{r}+\mathbf{a}) - \mathbf{E}_y(\mathbf{r})\right] - (ib)^{-1}\left[\mathbf{E}_x(\mathbf{r}+\mathbf{b}) - \mathbf{E}_x(\mathbf{r})\right] &= \omega\mathbf{B}_z(\mathbf{r}) \end{aligned} \tag{16}$$

and

$$\begin{aligned}
(ib)^{-1}\left[\mathbf{H}_z(\mathbf{r}+\mathbf{b})-\mathbf{H}_z(\mathbf{r})\right]-(ic)^{-1}\left[\mathbf{H}_y(\mathbf{r}+\mathbf{c})-\mathbf{H}_y(\mathbf{r})\right]&=\omega\mathbf{D}_x(\mathbf{r})\\
(ic)^{-1}\left[\mathbf{H}_x(\mathbf{r}+\mathbf{c})-\mathbf{H}_x(\mathbf{r})\right]-(ia)^{-1}\left[\mathbf{H}_z(\mathbf{r}+\mathbf{a})-\mathbf{H}_z(\mathbf{r})\right]&=\omega\mathbf{D}_y(\mathbf{r})\\
(ia)^{-1}\left[\mathbf{H}_y(\mathbf{r}+\mathbf{a})-\mathbf{H}_y(\mathbf{r})\right]-(ib)^{-1}\left[\mathbf{H}_x(\mathbf{r}+\mathbf{b})-\mathbf{H}_x(\mathbf{r})\right]&=\omega\mathbf{D}_z(\mathbf{r})
\end{aligned} \qquad (17)$$

Note that in (16) and (17) the time dependence is included in the **E** and **H** plane waves.

We now rewrite **B** and **D** in terms of **H** and **E**,

$$\mathbf{D}(\mathbf{r})=\varepsilon_0\varepsilon(\mathbf{r})\mathbf{E}(\mathbf{r}),\quad \mathbf{B}(\mathbf{r})=\mu_0\mu(\mathbf{r})\mathbf{H}(\mathbf{r}) \qquad (18)$$

Furthermore it is assumed that all cell dimensions are equal, such that b=c=a. This is of course not necessary, and it limits the solutions to cubic symmetries, but it brings out more clearly the interesting result below.

$$\begin{aligned}
\left[\mathbf{E}_z(\mathbf{r}+a)-\mathbf{E}_z(\mathbf{r})\right]-\left[\mathbf{E}_y(\mathbf{r}+a)-\mathbf{E}_y(\mathbf{r})\right]&=+ia\omega\mu_0\mu(\mathbf{r})\mathbf{H}_x(\mathbf{r})\\
-\left[\mathbf{H}_z(\mathbf{r}-a)-\mathbf{H}_z(\mathbf{r})\right]+\left[\mathbf{H}_y(\mathbf{r}-a)-\mathbf{H}_y(\mathbf{r})\right]&=-ia\omega\varepsilon_0\varepsilon(\mathbf{r})\mathbf{E}_x(\mathbf{r})
\end{aligned} \qquad (19)$$

$$\begin{aligned}
\left[\mathbf{E}_x(\mathbf{r}+a)-\mathbf{E}_x(\mathbf{r})\right]-\left[\mathbf{E}_z(\mathbf{r}+a)-\mathbf{E}_z(\mathbf{r})\right]&=+ia\omega\mu_0\mu(\mathbf{r})\mathbf{H}_y(\mathbf{r})\\
-\left[\mathbf{H}_x(\mathbf{r}-a)-\mathbf{H}_y(\mathbf{r})\right]+\left[\mathbf{H}_z(\mathbf{r}-a)-\mathbf{H}_z(\mathbf{r})\right]&=-ia\omega\varepsilon_0\varepsilon(\mathbf{r})\mathbf{E}_y(\mathbf{r})
\end{aligned} \qquad (20)$$

$$\begin{aligned}
\left[\mathbf{E}_y(\mathbf{r}+\mathbf{a})-\mathbf{E}_y(\mathbf{r})\right]-\left[\mathbf{E}_x(\mathbf{r}+a)-\mathbf{E}_x(\mathbf{r})\right]&=+ia\omega\mu_0\mu(\mathbf{r})\mathbf{H}_z(\mathbf{r})\\
-\left[\mathbf{H}_y(\mathbf{r}-\mathbf{a})-\mathbf{H}_y(\mathbf{r})\right]+\left[\mathbf{H}_x(\mathbf{r}-a)-\mathbf{H}_x(\mathbf{r})\right]&=-ia\omega\varepsilon_0\varepsilon(\mathbf{r})\mathbf{E}_z(\mathbf{r})
\end{aligned} \qquad (21)$$

Assuming the electromagnetic wave propagates in the z direction, use in (21) the equations for the longitudinal z components of the **E** and **H** field to reduce and rewrite (19) and (20). The component equations can now be rewritten using a *transfer matrix*:

$$\begin{bmatrix}\mathbf{E}_x(r+a)\\ \mathbf{E}_y(r+a)\\ \mathbf{H}_x(r+a)\\ \mathbf{H}_y(r+a)\end{bmatrix}=\sum_{r'}\begin{bmatrix}T_{11} & T_{12} & T_{13} & T_{14}\\ T_{21} & T_{22} & T_{23} & T_{24}\\ T_{31} & T_{32} & T_{33} & T_{34}\\ T_{41} & T_{42} & T_{44} & T_{44}\end{bmatrix}\cdot\begin{bmatrix}\mathbf{E}_x(r')\\ \mathbf{E}_y(r')\\ \mathbf{H}_x(r')\\ \mathbf{H}_y(r')\end{bmatrix} \qquad (22)$$

where the summation is over a discrete set of points in a plane. All matrix elements T_{nm} are functions of **r** and **r**'.

In the case where we have a periodic structure which repeats after L_z cells, the fields on each side of the unit cell can be related as such:

$$\begin{bmatrix} \mathbf{E}_x(r+L_z a) \\ \mathbf{E}_y(r+L_z a) \\ \mathbf{H}_x(r+L_z a) \\ \mathbf{H}_y(r+L_z a) \end{bmatrix} = \sum_{r'} T(L_z,0) \cdot \begin{bmatrix} \mathbf{E}_x(r') \\ \mathbf{E}_y(r') \\ \mathbf{H}_x(r') \\ \mathbf{H}_y(r') \end{bmatrix} \tag{23}$$

where

$$T(L_z,0) = \prod_{j=1}^{L_z} T(j, j-1) \tag{24}$$

Bloch's theorem is now applied,

$$\begin{bmatrix} \mathbf{E}_x(r+L_z a) \\ \mathbf{E}_y(r+L_z a) \\ \mathbf{H}_x(r+L_z a) \\ \mathbf{H}_y(r+L_z a) \end{bmatrix} = \exp(iK_z L_z a) \cdot \begin{bmatrix} \mathbf{E}_x(r) \\ \mathbf{E}_y(r) \\ \mathbf{H}_x(r) \\ \mathbf{H}_y(r) \end{bmatrix} \tag{25}$$

and the Bloch waves are identified as the eigenvectors of the transfer matrix.

$$\sum_{r'} T(L_z,0) \cdot \begin{bmatrix} \mathbf{E}_x(r') \\ \mathbf{E}_y(r') \\ \mathbf{H}_x(r') \\ \mathbf{H}_y(r') \end{bmatrix} = \exp(iK_z L_z a) \cdot \begin{bmatrix} \mathbf{E}_x(r) \\ \mathbf{E}_y(r) \\ \mathbf{H}_x(r) \\ \mathbf{H}_y(r) \end{bmatrix} \tag{26}$$

Thus, we can find all the Bloch waves for any given frequency. The advantage with the transfer matrix method described above, is that it calculates $\mathbf{k}(\mathbf{E},\varepsilon(\omega,\mathbf{r}))$ instead of $\mathbf{E}(\mathbf{k},\varepsilon(\omega,\mathbf{r}))$; in the latter case, the calculations are not straight forward due to the frequency dependence of ε: a recursive method must be used to obtain the result, which is numerically instable and tedious. With the method described above, we can obtain the band structure by

straight forward calculations, even when a true dispersion model for a dielectric - such as the Lorentz or Drude model - is included [9].

3.2 Calculating the transmittance

The transfer matrix equation (22) can be rewritten in a more compact notation,

$$F(z+a) = T(z)F(z) \tag{27}$$

where

$$F(z) = \begin{bmatrix} \mathbf{E}_x(r) \\ \mathbf{E}_y(r) \\ \mathbf{H}_x(r) \\ \mathbf{H}_y(r) \end{bmatrix} \tag{28}$$

T is not an Hermitian matrix, but can be transformed into one through a change of basis:

$$STS^{-1} = \begin{bmatrix} \exp(ik_1 a) & & & & 0 \\ & \exp(ik_2 a) & & & \\ & & \exp(-ik_1 a) & & \\ & & & \exp(-ik_2 a) & \\ 0 & & & & \ldots \end{bmatrix} \tag{29}$$

Here, S is a matrix used for the basis change, defined by normalizing (28) and component-wise multiplying F by its transponate. This new matrix is Hermitian, with the eigenvalues as the diagonal elements. For every eigenvalue $\exp(ik_j a)$ there is a second corresponding eigenvalue $\exp(-ik_j a)$, and the interpretation of these two eigenvalues is that the eigensolutions are waves travelling in opposite directions.

We can now use (29) to calculate transmission and reflection coefficients of a single layer of unit cells, referred to as a *slice*. Consider the new transfer matrix as given by (29) and rewrite it as

$$ST(z)S^{-1} = \hat{T}(z) = \begin{bmatrix} \hat{T}^{++}(z) & \hat{T}^{+-}(z) \\ \hat{T}^{-+}(z) & \hat{T}^{--}(z) \end{bmatrix} \tag{30}$$

The interpretation of (30) can be seen in figure 3 below: a wave incident from the right in the figure results in reflected and transmitted waves. $\mathbf{F}_{j'}^{-}$ represents a wave propagating from right to left and $\mathbf{F}_{j'}^{+}$ is a wave propagating from left to right; the - and + indicates the direction of propagation. As for the t-coefficients, -- or ++ indicates a transmitted wave from right to left and left to right, respectively, and +- or -+ indicates a reflected wave propagating from left to right and right to left, respectively.

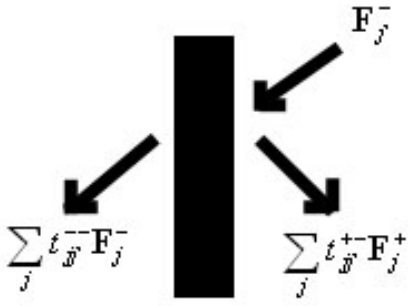

Fig. 3: A wave, $\mathbf{F}_{j'}^{-}$, incident from the right on a slice results in a transmitted wave, $\sum_j t_{jj'}^{--}\mathbf{F}_j^{-}$, and a reflected wave, $\sum_j t_{jj'}^{+-}\mathbf{F}_j^{+}$.

Using the transfer matrix, we can start with the waves on the left hand side of the system, i.e. the transmitted wave,

$$\sum_j t_{jj'}^{--} F_j^{-} \tag{31}$$

and integrate through the slice to obtain the amplitudes of the right hand waves:

$$\begin{bmatrix} t^{+-} \\ 1 \end{bmatrix} = \begin{bmatrix} \hat{T}^{++}(z) & \hat{T}^{+-}(z) \\ \hat{T}^{-+}(z) & \hat{T}^{--}(z) \end{bmatrix} \cdot \begin{bmatrix} 0 \\ t^{--} \end{bmatrix} \tag{32}$$

from which can be obtained

$$\begin{aligned} \hat{T}^{+-}(z) &= t^{+-}(t^{--})^{-1} \\ \hat{T}^{--}(z) &= (t^{--})^{-1} \end{aligned} \tag{33a, b}$$

The other two components of the matrix in (32) are found if the waves on the left hand side are observed,

$$\sum_j t_{jj'}^{++}\mathbf{F}_j^+ + t_{jj'}^{-+}\mathbf{F}_j^- \tag{34}$$

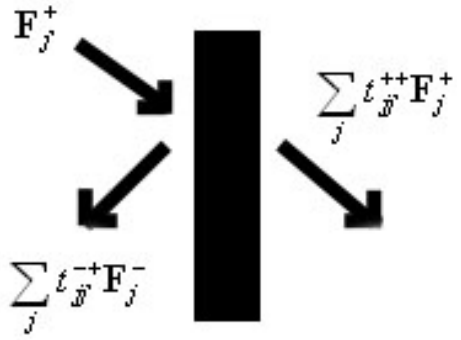

Fig. 4: A wave incident from the left, $\mathbf{F}_{j'}^+$, results in a reflected wave, $\sum_j t_{jj'}^{-+}\mathbf{F}_j^-$, and a transmitted wave, $\sum_j t_{jj'}^{++}\mathbf{F}_j^+$

and as above, we integrate through the slice to obtain

$$\begin{bmatrix} t^{++} \\ 0 \end{bmatrix} = \begin{bmatrix} \hat{T}^{++}(z) & \hat{T}^{+-}(z) \\ \hat{T}^{-+}(z) & \hat{T}^{--}(z) \end{bmatrix} \cdot \begin{bmatrix} 1 \\ t^{-+} \end{bmatrix} \tag{35}$$

which results in

$$\begin{aligned} \hat{T}^{++}(z) &= t^{++} - t^{+-}(t^{--})^{-1}t^{-+} \\ \hat{T}^{-+}(z) &= \qquad -(t^{--})^{-1}t^{-+} \end{aligned} \tag{36a, b}$$

Now, we can summarize equations (33a,b) and (36a,b) into

$$\hat{T} = \begin{bmatrix} \hat{T}^{++}(z) & \hat{T}^{+-}(z) \\ \hat{T}^{-+}(z) & \hat{T}^{--}(z) \end{bmatrix} = \begin{bmatrix} t^{++} - t^{+-}(t^{--})^{-1}t^{-+} & t^{+-}(t^{--})^{-1} \\ -(t^{--})^{-1}t^{-+} & (t^{--})^{-1} \end{bmatrix} \tag{37}$$

which is a matrix fully describing the transmission through a slice of the material.

By putting several slices together, we get a thicker unit, a *slab*, of the material. Since the transfer matrix starts with the calculated **E** and **H** fields defined in a slice and then integrates through to the next slice, it is straight-forward to stack multiple slices together by defining a new transfer matrix that is the product of the transfer matrices for each slice:

$$T(L_z) = \prod_{z=1}^{L_z} T(z) \tag{38}$$

which used as a substitute for T(z) in (30) gives

$$ST(L_z)S^{-1} = \hat{T}(L_z) = \begin{bmatrix} t_{L_z}^{++} - t_{L_z}^{+-}(t_{L_z}^{--})^{-1} t_{L_z}^{-+} & t_{L_z}^{+-}(t_{L_z}^{--})^{-1} \\ -(t_{L_z}^{--})^{-1} t_{L_z}^{-+} & (t_{L_z}^{--})^{-1} \end{bmatrix}, \tag{39}$$

a matrix from which we can obtain the transmission coefficients for the entire slab of the material.

4. Calculations

4.1 2D structure of dielectric cylinders in air

We have calculated the photonic band structure for a bulk 2D crystal with a square lattice of dielectric cylinders, $\varepsilon = 8.9$, embedded in air ($\varepsilon = 1$). The cylinders are oriented in the y-direction, as indicated in figure 5 below. This is similar to a case studied earlier by Joannopoulos et al [10].

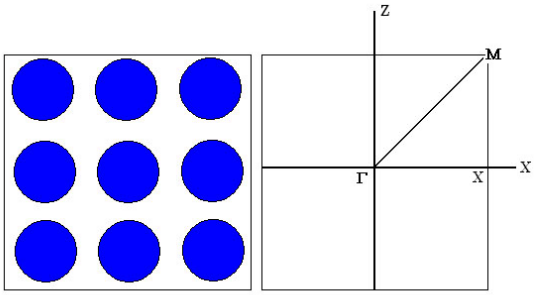

Fig. 5: A cross-section of the quadratic structure of cylinders (left) and the Brillouin zone (right) with the high symmetry points. It should be noticed that the Brillouin zone is the unit cell in reciprocal space, “k-space”, and in the case of a square lattice the Brillouin zone is also a square. The y axis is perpendicular to the paper plane.

The ratio between the cylinder radius and the cell constant has been chosen as r/a = 0.2, and the unit cell length is set to a = 1.0 µm. The band structure, obtained as described in the previous section, is shown below in figure 6 where the transverse electric (TE, red) and transverse magnetic (TM, blue) modes for the high symmetry directions in the Brillouin zone, where TE and TM modes are characterized by having the electric and the magnetic field vector, respectively, perpendicular to the cylinders, i.e. the y-axis in figure 5.

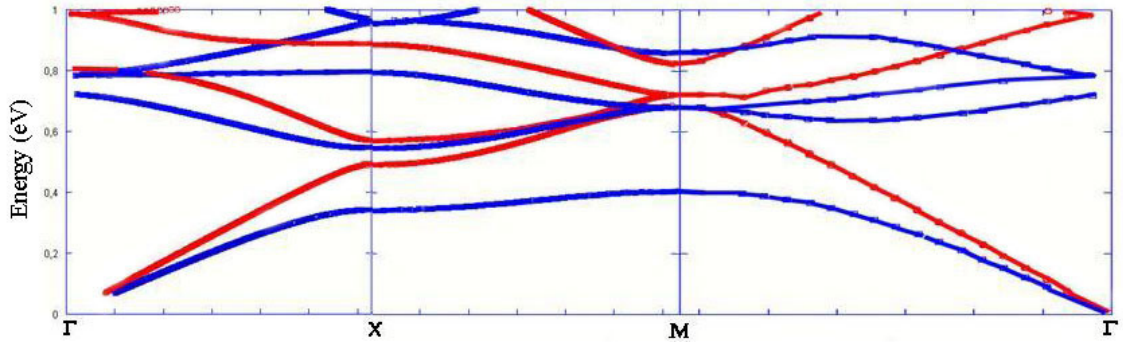

Fig. 6: The photonic band structure for the two-dimensional square array of cylinders (ε=8.9) embedded in air, with the lattice constant a=1.0µm. The photon energy is in eV.

In the band structure, we note the absence of a complete photonic band gap, i.e. in all directions, for both polarizations, even though there are separate gaps for s- and p-polarized light within the Brillouin zone. For normal incidence, corresponding to the Γ-X part of the band structure, we have band gaps for TE modes as well as for TM modes but at different energies. It can be qualitatively understood from observing the behaviour of the dielectric displacement field within the material. The **D**-field is strongly concentrated to the regions where ε is high, i.e. the cylinders, since the **D**-field is directly proportional to the dielectric function. One mode concentrates most of the displacement energy within the cylinders, which is beneficial from an energy point of view, which lowers the energy of the mode. The first TM band, the band of lowest energy (the *dielectric band*) has most power in the dielectric cylinders, and the second TM band (the *air band*) has most of the power in the air surrounding the cylinders. This is what causes the bands to split. For the TE bands, the difference between power transmitted through the cylinders and through the surrounding air is not as large as for the TM modes, since the air in the material is not as well localized as the dielectric. This gives only a small TE band gap.

In the transmittance spectrum below calculated with (39), for normal incidence, corresponding to the X point of the band structure, it can clearly be seen that the gaps for TE and TM modes only have a small overlap. The thickness of this structure is 8 μm.

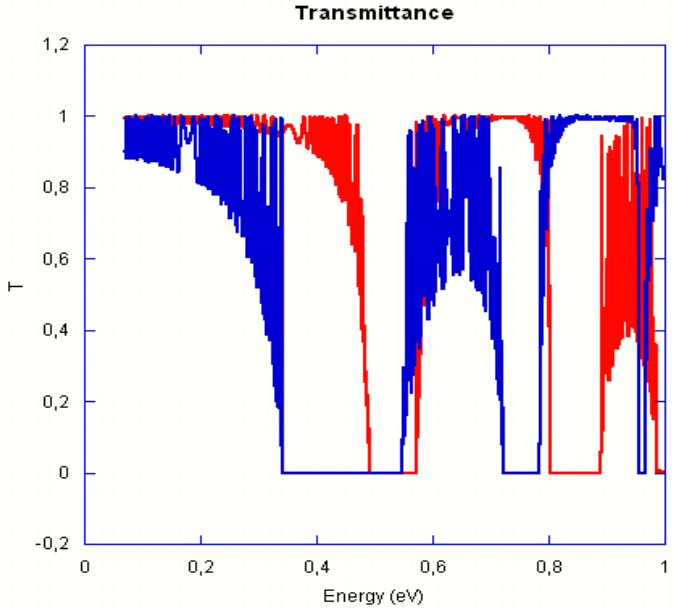

Fig. 7: Transmittance for normal incidence. Note the small region where T=0 for both TE and TM modes. The slab thickness is 8μm.

Focussing onto the Γ-X part of the band structure, the behaviour of the band structure can be further investigated by changing one of the parameters. By varying the packing fraction, r/a, from 0.1 up to 0.5 - the upper limit corresponding to touching cylinders - we can see that there is a value near the originally r/a value, 0.2, for which the band gaps have maxima, and also that the TM gap width decreases sharply from its maximum for other packing fraction values. The fact that both gaps have maxima does not imply that they overlap, as seen in figure 9, which shows the TM and TE dielectric and air bands. However, one should note the striking difference in behaviour of the TE and TM gaps. In figure 8 below one can note that the TE gaps are less sensitive, in comparison with the TM gaps, to changes in packing fraction.

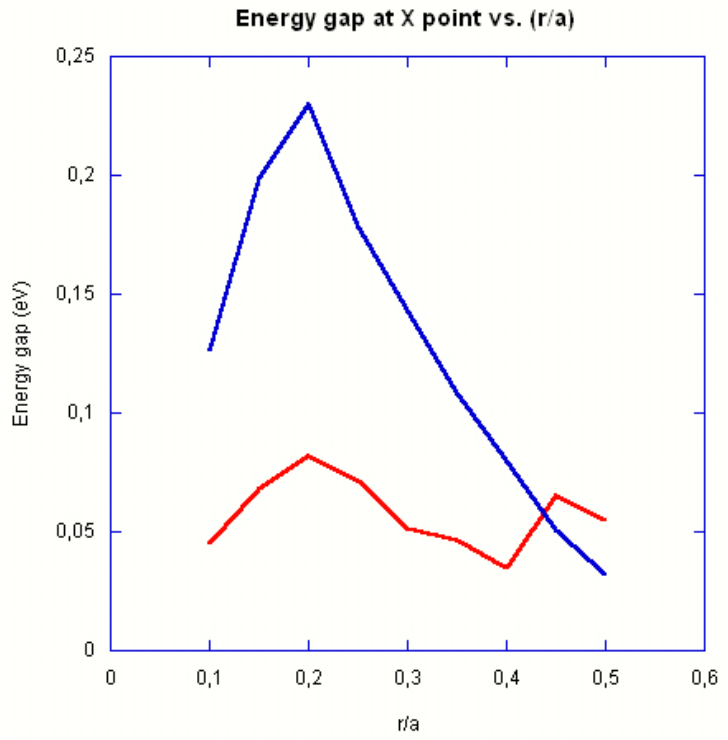

Fig. 8: The size of the band gap, for TE and TM modes, as a function of the packing fraction.

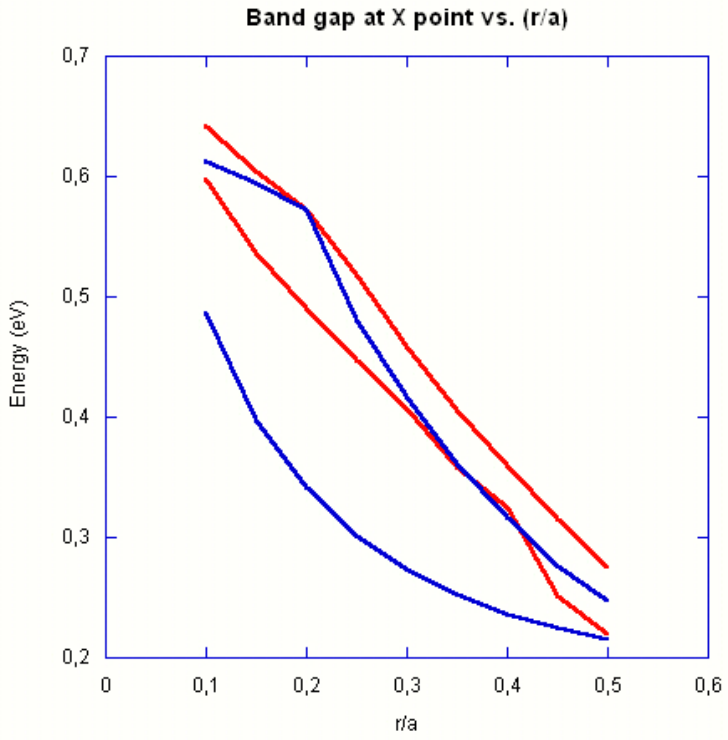

Fig. 9: The TE (red) and TM (blue) dielectric and air bands at the X point, showing the band gap as a function of packing fraction. It should be noticed that the gaps only partly overlap within narrow energy intervals.

Figure 10 shows the midgap energy as a function of the packing fraction, and it can be observed that as the packing fraction decreases, the midgap energy increases, which means that the band gap, and thus the highly reflective region, moves towards shorter wavelengths. This gives a possibility to use different packing fractions and thus tailor the material to be highly reflective in specified regions. However, also the results shown in figure 8 and 9 above should be remembered. A packing fraction of 0.2 gives, for TE as well as TM modes, the widest gap centred around 0.45 eV and 0.53 eV respectively, but the band gaps for TE and TM modes only overlap partly since the TM gap is wider.

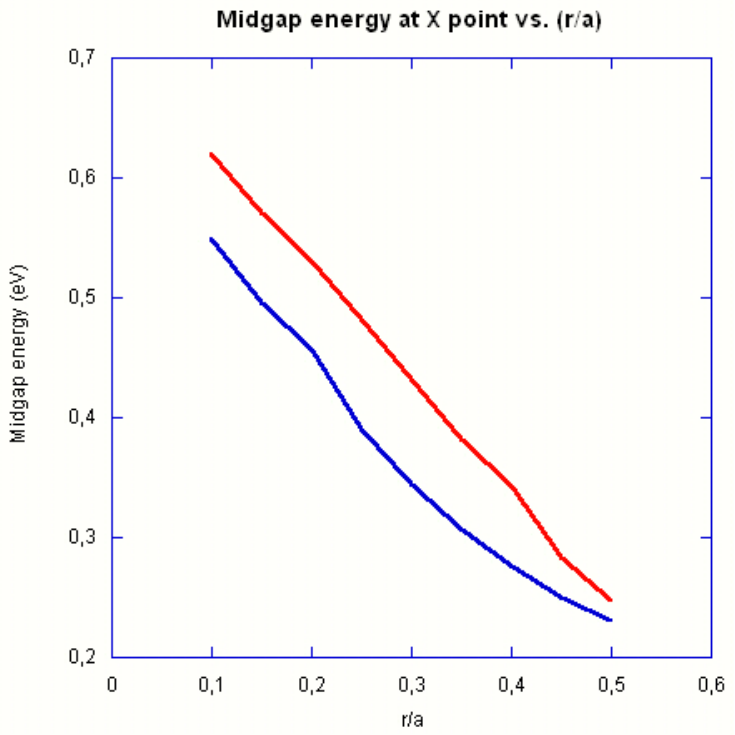

Fig. 10: The midgap energy of the band gap as a function of the packing fraction.

4.2 2D structure of air cylinders in a dielectric medium

We have also studied the inverse of the above structure: a bulk 2D crystal created from a square array of air holes, or 'wells', in a dielectric (ε=8.9). Here, the structure is close-packed (r/a=0.5), and the wells are, as in the previous case, oriented in the y-direction. The band structure below is not complete in the M-Γ part; there is a TM mode missing due to numerical problems in the calculations. As in figure 6, red lines are the TE modes, and blue the TM modes, and the points of high symmetry are indicated on the x-axis.

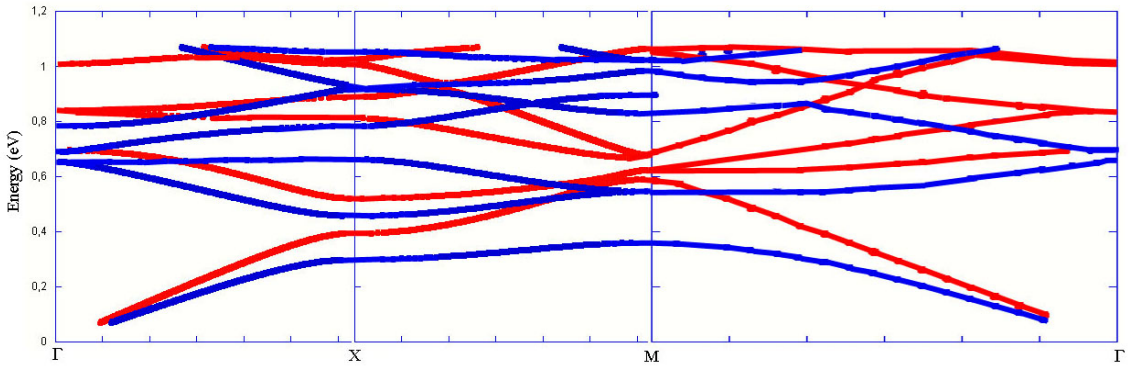

Fig. 11: The photonic band structure for the two-dimensional square array of close-packed (r/a = 0.5) air wells in a dielectric (ε=8.9), with red TE modes and blue TM modes.

As for the previous case, there is no complete band gap for this structure. The transmittance, for normal incidence at the X point of the band structure, was calculated for the case of close-packed air holes. The thickness of this structure is also 8 μm. Some very dense interference fringes can be observed in the lower energy part of the spectrum, and the energies where T=0 clearly correspond to the band gaps at the X point in figure 11.

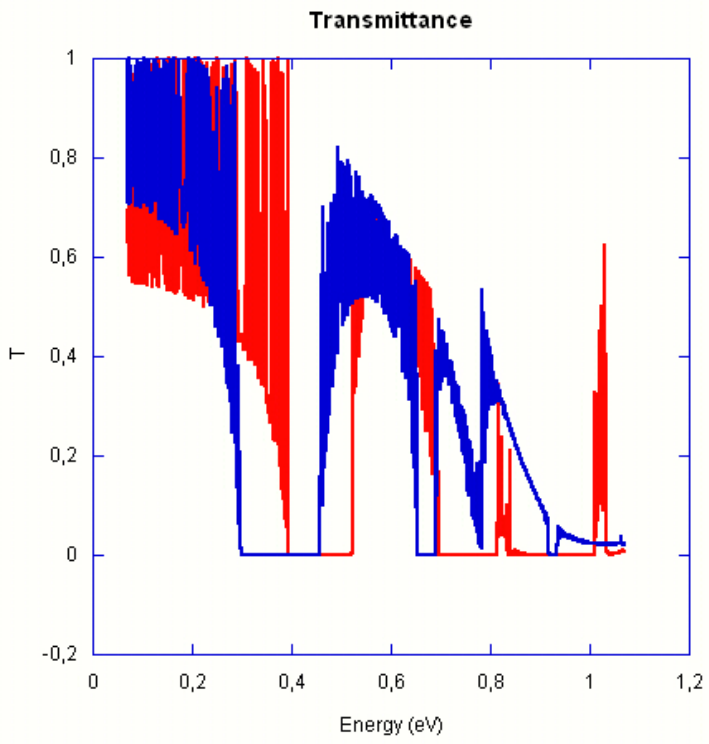

Fig. 12: Transmittance for normal incidence, corresponding to the Γ-X part of the band structure.

Also, in this case we have calculated the band gap width as a function of the packing fraction. Compared to the previous case, one should note that the gap widths tend to increase with the packing fraction instead of having a distinct optimum value as seen in figure 8, and also that

both TE and TM gaps are more sensitive to changes in r/a. The reason for this may be that the difference in the amount of dielectric present in the material. In the first case, the volume fraction of dielectric is 0.126, and for the second case it is 0.214. The amount of dielectric medium in the material affects the energy flow; as mentioned earlier the displacement field is proportional to the dielectric function, and thus the displacement is larger in the areas where ε is high, which lowers the frequency. As the volume fraction of the dielectric medium increases, the more power is within the TM dielectric bands.

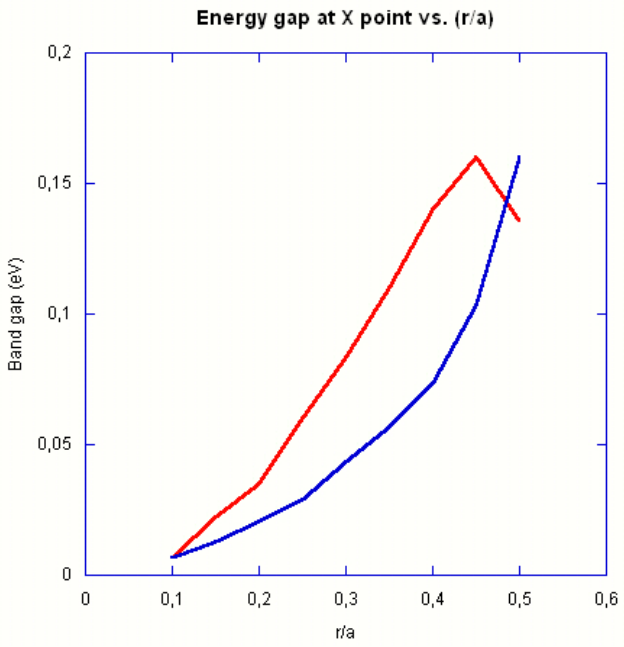

Fig. 13: The photonic band gap width as a function of the packing fraction, for the square lattice of air holes.

In figure 13 it is seen that the band gap tends to move towards higher energies, i.e. shorter wavelengths, as the packing fraction is increased.

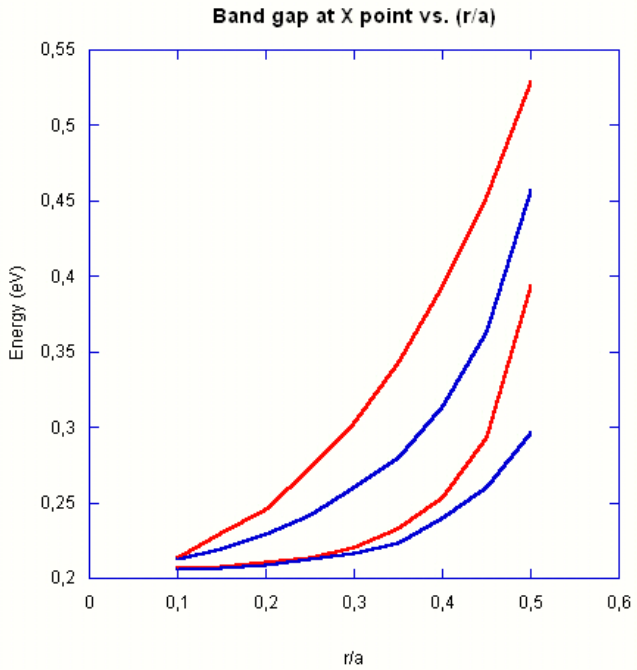

Fig. 14: The TE (red) and TM (blue) dielectric and air bands, at the X-point of the band structure in figure 11. Note that the band gaps for TE and TM modes overlap partly, regardless of the packing fraction r/a.

The midgap energy was studied as well, and found to behave differently from the previous case. For this structure the midgap energy increases with increasing packing fraction.

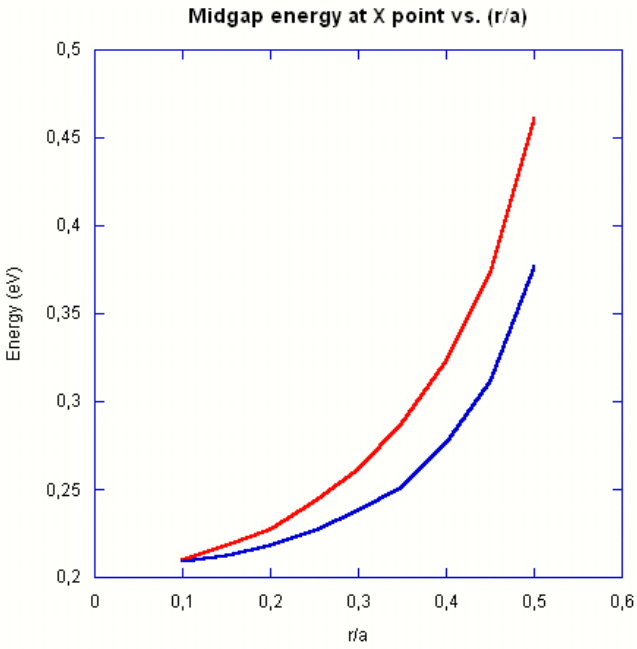

Fig. 15: The midgap energy for TE and TM mode band gaps at the X-point.

If the topology of the two structures is compared, it is noticed that in the first case we have cylindrical 'islands' where ε is high, and in the second case we have a connected structure,

with ‘islands’ of air. If the band structures are examined for the two cases, it is observed that for the first structure, the TM band gap is generally wider than the TE band gap, and vice versa for the latter case. This phenomenon can be qualitatively understood from the behaviour of the **D**-field within the material. In the case where the high ε regions are localized to cylinders, the **D**-field is forced to propagate through air, due to a continuity constraint on the field lines, even though propagating through the cylinders are beneficial from an energy point of view. This results in the power being concentrated to the dielectric regions, which lowers the frequency of the TM dielectric mode as described earlier. In the second case, where the *air* regions are localized to cylinders, the **D**-field prefers to propagate outside the air cylinders, and thus the TM modes are localized to the high ε region. Here, the field lines are not forced to propagate through air, which makes the energy more evenly distributed in the material. The TE modes are localized to the air cylinders, and the localization gives rise to the same effect as for the TM modes in the first case; the frequency for the TE dielectric band is lowered, and thus the gap becomes widened.

5. Conclusions

In this work we have described the fundamentals of photonic crystals, as well as one method for calculating a photonic band structure: the transfer matrix method. A software package was used to obtain band structures for two photonic band gap materials: one consisting of dielectric cylinders in a square lattice, and one with drilled holes in a dielectric medium. The band structures for these two-dimensional photonic crystals were presented, as well as optical transmittance spectra for the case of normal incidence. Also, the photonic band gap width was presented as a function of the packing fraction, r/a, of cylinders and holes.

In the band structures we noticed the absence of complete photonic band gaps, but also the presence of TE and TM gaps for certain crystallographic directions. By modulating the packing fraction, we observed for the first material – the dielectric cylinders in air – that there was an optimum value for r/a, close to 0.2. No distinct optimum was found for the second material, the drilled holes in a dielectric.

From the transmittance calculations we observed that for normal incidence there are energy intervals where the transmittance, and thus the emittance, was zero. It should be noticed, however, that the zero transmittance intervals generally do not overlap for TE and TM modes.

6. References

1. J. D. Joannopoulos, R. D. Meade, J. N. Winn, ”Photonic crystals: Molding the Flow of Light”, Princeton Univ. Press, Singapore (1995).

2. W. L. Wolfe in “The Infrared handbook”(Ed’s W.L. Wolfe, G. J. Zissis, IRIA Ctr. ERIM, Office of Naval Research, Washington DC 1989) ch. 1, sec. 6k

3. R. Measures, “Laser Remote Sensing”, Wiley Interscience, J. Wiley & Sons (1984)

4. A. Rung, CG. Ribbing, “Calculated photonic structures for infrared emittance control”, Appl. Opt. 41, 3327-3331 (2002)

5. P. Lalanne,”Effective medium theory applied to photonic crystals composed of cubic or square cylinders. Appl. Opt. 35, 5369-5380 (1996)

6. P. M. Bell, J. B. Pendry, L. M. Moreno, A.J. Ward, ”A program for calculating photonic band structures and transmission coefficients of complex structures”, Computer Physics Commun. 85, 306-322 (1995)

7. J. B. Pendry, “Photonic band structures”, J. Mod. Opt. 41, no.2, 209-229 (1994)

8. J. B. Pendry, “Calculating photonic band structure”, J. Phys. Condens. Matter, 8, 1085-1108 (1996)

9. M. M. Sigalas, C. M. Soukoulis, C. T. Chan, K. M. Ho, “Electromagnetic wave propagation through dispersive and absorptive photonic band gap materials”, Phys. Rev. B, 49, 11080-11087 (1994)

10. As ref. 1, ch. 5, p. 56.